ACS OMEGA

Open Access

http://pubs.acs.org/journal/acsodf

Article

High-Quality Thiophene-Based Two-Dimensional Perovskite Films Prepared with Dual Additives and Their Application in Solar Cells

Xiaoyan Gan,* Kegui Li, Longtao Du, Ruoqi Wang, Yuge Chang, Liling Guo, and Hanxing Liu

Cite This: *ACS Omega* 2024, 9, 46006−46016

Read Online

ACCESS | Metrics & More | Article Recommendations | Supporting Information

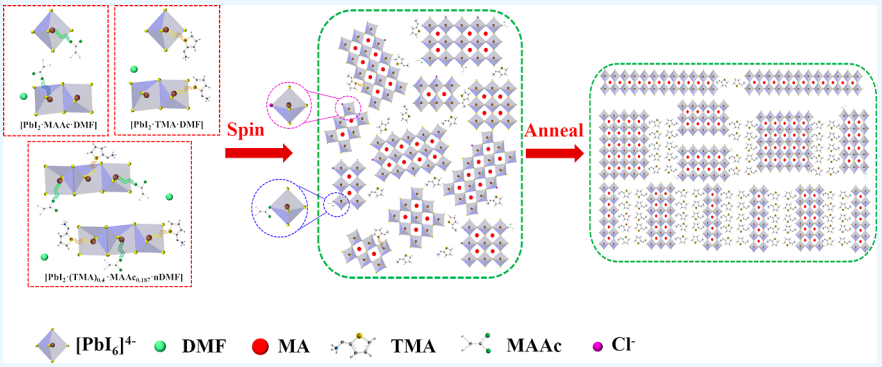

ABSTRACT: This study explores the optimization of $(TMA)_2MA_4Pb_5I_{16}$ perovskite films by regulating the film quality through the addition of MACl and MAAc additives. We found that adding MACl resulted in a film of larger grains with a power conversion efficiency (PCE) of 5.34%, while excessive MACl led to the formation of low-dimensional phases. Adding 7.5% MAAc improved the film quality with a PCE of 5.64%, although excessive MAAc induces pores and smaller grains. To address these issues, we proposed the combined use of MACl and MAAc additives, resulting in films with a larger grain size, smoother surface, and denser structure. Remarkably, the addition of MAAc + MACl achieved a champion PCE of 8.86% with good reproducibility. Mechanism studies revealed that TMA and MAAc formed a stable complex with PbI_2 in solution, disrupting nucleation laws and promoting the formation of nuclei, leading to denser films with smaller grains. Additionally, the MACl treatment effectively promoted grain growth, resulting in high-quality films. This study presents novel insights into dual additive usage and their role in film crystallization, offering valuable guidance for the preparation of high-performance perovskite films.

INTRODUCTION

The rapid development of perovskite solar cells (PSCs) in recent years has attracted widespread attention.[1,2] However, the instability of the three-dimensional (3D) perovskite structure significantly limits its commercial applications.[3−5] In contrast, quasi-two-dimensional (2D) PSCs have emerged as a key solution to this issue due to their excellent stability, high structural versatility, and tunable optoelectronic properties.[6−9] Achieving high-performance quasi-2D PSCs places particularly emphasis on the quality of perovskite films.[10−12] Over recent years, several methods have been developed to optimize perovskite film quality, such as thermal casting,[13−15] antisolvent methods,[16−18] and additive methods.[19−22] Among these methods, thermal casting requires precise control over the substrate temperature. However, issues with substrate transfer commonly result in temperature losses during the experiment, leading to poorer film quality.[23] The antisolvent method involves a narrow operation window of antisolvent quantity and addition time, requiring extensive trial and error to determine suitable parameters.[24] Therefore, these two preparation methods are challenging to replicate consistently. In contrast, the additive method involves adding a specific amount of additive to the precursor solution, leveraging the additive's high volatility during spin-coating to preserve the original perovskite structure and achieve high-quality perovskite films.[25,26] Due to its simplicity, high repeatability, and low manufacturing costs, the additive method has been widely adopted.[27,28]

In recent years, the additive method has been widely applied in the preparation of quasi-2D PSCs. For instance, in 2018, Lai et al.[29] achieved dense nanorod-shaped films by regulating the growth of $ThMA_2(MA)_2Pb_3I_{10}$ using methylammonium chloride (MACl), resulting in a remarkable enhancement of the device's power conversion efficiency (PCE) from 1.74 to

Received: June 25, 2024
Revised: October 25, 2024
Accepted: October 29, 2024
Published: November 5, 2024

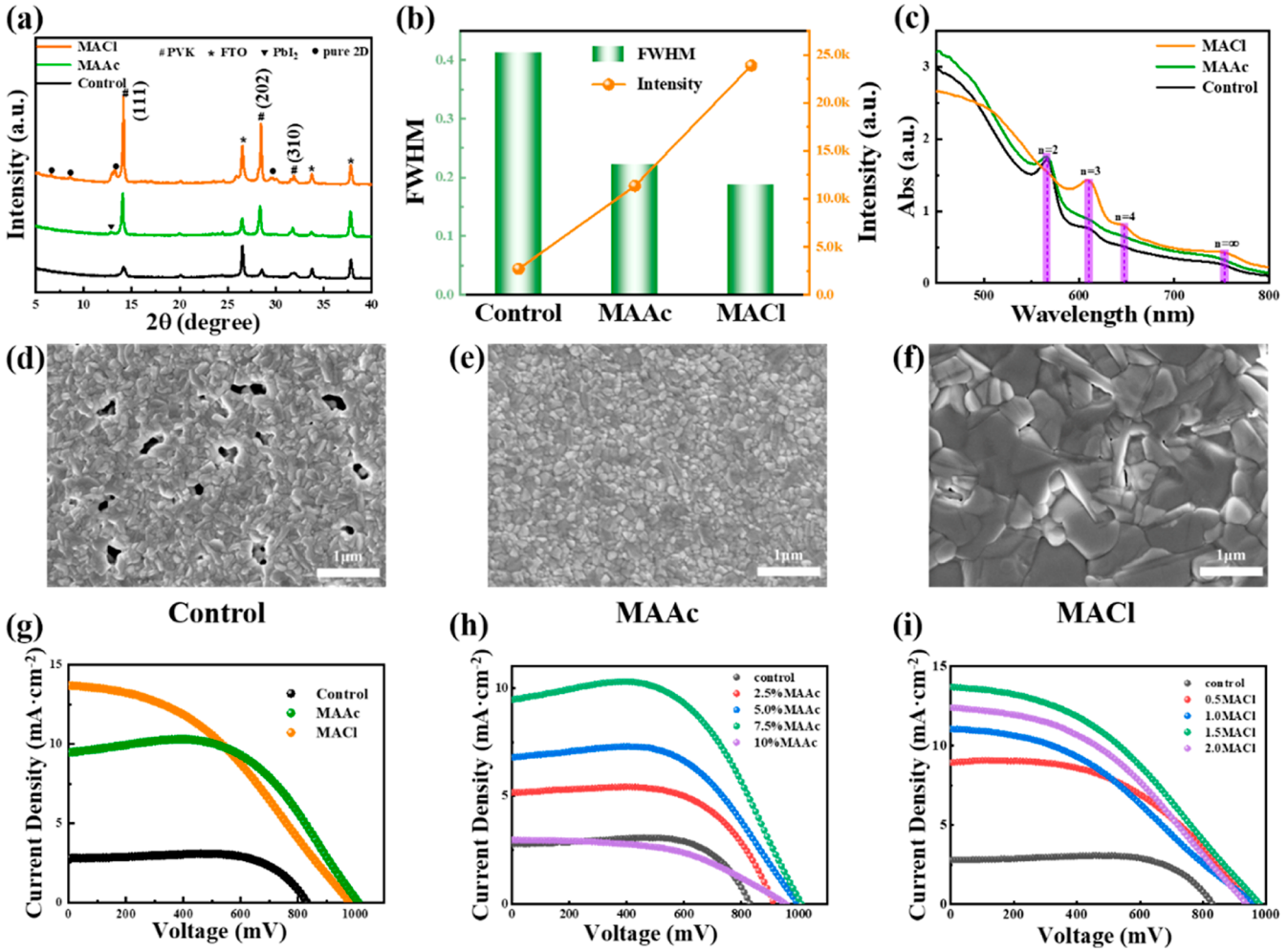

Figure 1. (a) XRD spectra of a single additive; (b) corresponding peak width and intensity of the (111) crystal plane; (c) UV−vis absorption spectra of a single additive; (d−f) top-view SEM images of films without additives (d) and with added MAAc (e) and MACl (f); and (g) optimal performance *J*−*V* curve of a single additive. (h−i) *J*−*V* curves of different contents of MAAc (h) and MACl (i) added. To investigate the morphological effects of different additives on the $(TMA)_2(MA)_4Pb_5I_{16}$ film, SEM testing was conducted, as shown in Figure 1d−f. In the absence of additives, numerous pores were observed on the film surface, accompanied by small grain sizes, indicative of poor film quality. Upon addition of MAAc, the number of surface pores decreased, leading to an improvement in film quality. With the addition of MACl, a reduction in surface pores was observed, accompanied by an increase in grain size and an enhancement in film quality. When different concentrations of MAAc were added, it was found that at 5% and 7.5% concentrations, the film surface appeared (Figure S3) dense and smooth, with distinct grain boundaries, albeit with smaller grain sizes. Further addition of MAAc resulted in the appearance of significant pores. Upon addition of MACl (as shown from the SEM images in Figure S4), the grain size further increased, accompanied by the emergence of distinct lamellar grains, indicative of the generation of a significant amount of low-dimensional phase crystals, consistent with the XRD analysis. Upon addition of 1.5MACl, the lamellar crystals decreased, leading to a denser film with overall improved quality. However, upon further addition of 2MACl, a resurgence of lamellar crystals was observed, accompanied by significant pores, demonstrating a decreased quality of the film.

15%. In 2022, Xu et al.[30] introduced methylamine acetate (MAAc) into the precursor to prepare $(BPEA)_2(MA)_4Pb_5I_{16}$ films, leading to a PCE of 8.47%, significantly higher than devices without MAAc (4.79%). In 2023, Lu et al.[31] utilized NH_4SCN to modulate $(FPEA)_2(MA)_4Pb_5I_{16}$ films, obtaining highly crystalline and smooth perovskite films. Further doping with FA^+ resulted in a PCE of 12.17%. Moreover, previous studies have shown that the performance of devices using dual additives surpasses those with a single additive.[32] For instance, in 2018, Fu et al.[33] achieved a stable PCE of 14.1% by employing NH_4SCN and NH_4Cl as dual additives in the preparation of $(PEA)_2(MA)_4Pb_5I_{16}$ films, producing highly crystalline films with a vertical orientation, far exceeding devices with single additives. In 2019, Yan et al.[34] improved the crystallinity and orientation of perovskite films by using NH_4Cl and dimethyl sulfoxide as dual treatments during the preparation of $(TEA)_2(MA)_3Pb_4I_{13}$ films, increasing the PCE from 7.2 to 11%. Although many additives have been proven to improve film quality, their function mechanism, especially the function mechanism of multiadditive, has not been thoroughly studied. Moreover, there is still controversy over the types and contents of additives used in the preparation of TMA-based perovskite films, and most of them are single additives. Therefore, exploring which additives are more suitable for TMA-based 2D PSCs is of great significance.

In recent years, thiophene methylamine (TMA) not only has excellent hydrophobic properties but also the presence of high polarization sulfur atoms makes it highly efficient in carrier transport when applied to 2D PSCs and has been widely used in 2D PSCs.[35−38] In this study, MACl and MAAc were selected

https://doi.org/10.1021/acsomega.4c05875
ACS Omega 2024, 9, 46006−46016

as additives to investigate the influence of additives on the quality of the $(TMA)_2(MA)_4Pb_5I_{16}$ perovskite films. On quasi-2D perovskite films, a synergistic effect of dual additives (MACl + MAAc) was observed to achieve high-quality perovskite films. Compared to single additives, the films obtained with dual additives exhibited stronger crystallinity, larger grain size, and better uniformity. The PCE of PSCs based on $(TMA)_2(MA)_4Pb_5I_{16}$ films increased from 5 to 8.83%. The interactions between the reactants and MAAc were further studied, and the formation mechanism of quasi-2D perovskites in the presence of the dual additives was proposed, offering fresh insights for the fabrication of high-quality perovskite films.

EXPERIMENTAL DETAILS

Materials. Methylamine hydroiodide (MAI, ≥99.5%), PbI_2(≥99.9%), Spiro-OMeTAD (99.5%), and $PC_{61}BM$ (≥99%) were bought from Xi'an Yuri Solar co., Ltd. 2-Thiophenemethylamine (97%) and HI aqueous solution (55−58% w/w) were bought from Aladdin. Titanium(IV) chloride (98%) was purchased from Sinopharm Chemical Reagent Co, Ltd. *N*,*N*-Dimethylformamide (99.8%) and chlorobenzene (99.8%) were bought from Sigma-Aldrich.

Solubility Test. The testing temperature ranges from 25 to 100 °C. The testing process refers to the method reported in the literature.[1] 1 mL of DMF was taken as the solvent, heated to the desired temperature, and a small amount of PbI_2 (0.01 g each time) was added multiple times until the solution reached saturation. When the solute remained insoluble within 10 min, it was considered saturated, and the solubility curve was finally obtained.

Device Fabrication. The FTO glass substrate was sequentially ultrasonicated for 15 min in detergent, deionized water, and anhydrous ethanol. The cleaned glass was dried and subjected to an oxygen plasma treatment for 15 min. The electron transport layer TiO_2 was prepared using a chemical deposition method. The glass was immersed in 100 mL of a 0.002 M $TiCl_4$ aqueous solution and maintained at 70 °C for 20 min. After the sample was rinsed with ultrapure water and dried, the above procedure was repeated with a fresh $TiCl_4$ solution. The dried glass was heated to 450 °C in 30 min, kept it warm for 30 min, and then naturally cooled it to room temperature. Before the perovskite was spin-coated, the FTO/TiO_2 substrate was treated with UV ozone for 15 min. The perovskite layer was spin-coated onto the FTO/TiO_2 substrate by using a one-step deposition method. The precursor solution for the perovskite consisted of TMAI, MAI, PbI_2, and MAAc/MACl in a ratio of 2:4:5:x/y (x = 2.5−10%; y = 0.5−2), with Pb^{2+} concentration controlled at 1 M in DMF. After stirring the precursor solution for 4 h, the solution was filtered using a polytetrafluoroethylene (PTFE) filter (0.22) before spin coating. Then, 35 μL of precursor solution was evenly dripped onto the FTO/TiO_2 substrate and rotated at 4000 rpm for 40 s, and the film was quickly annealed at 100 °C for 30 min. The hole transport layer was prepared by dissolving 83.2 mg Spiro-OMeTAD, 34 μL TBP, 16 μL Li-TFSI (dissolved in acetonitrile at a concentration of 0.5 g/mL), and 14 μL FK209 (dissolved in acetonitrile at a concentration of 0.2 mg/mL) in 1 mL of chlorobenzene. The mixture solution was spin-coated on the quasi-2D perovskite at 3000 rpm for 30 s. The deposition of perovskite films and hole transport layer was conducted in a N_2-filled glovebox. Finally, 80 nm gold electrode was deposited on the hole transport layer substrate using thermal evaporation.

Characterization. The X-ray diffraction (XRD) patterns were acquired using a PANalytical X'Pert PRO X-ray diffractometer. The field emission scanning electron microscopy (FE-SEM, Zeiss Ultra Plus, Germany) was utilized to capture surface and cross-sectional morphology images. The analysis of the UV−visible absorption spectrum was conducted using a UV−vis−NIR spectrophotometer (PerkinElmer Lambda 750 s, US). The steady-state photoluminescence (PL)spectra were obtained by using a PL microscopic spectrometer (FL3−22, Jobin Yvon, France). Functional groups are tested by FTIR (Thermo Nicolet Nexus, US). Photocurrent density−photovoltage (J−V) curves were gained under lighting from an Air Mass 1.5 Global (AM 1.5) solar simulator (Oriel 94023A, US) with an intensity of irradiation of 100 mW·cm^{-2}.

RESULTS AND DISCUSSION

Influence of Single Additives on the Quality of Thin Films. To investigate the impact of additives on the $(TMA)_2(MA)_4Pb_5I_{16}$ film, MACl and MAAc were separately employed as additives. As illustrated in Figure 1a, upon the addition of additives, characteristic perovskite diffraction peaks of (111) and (202) emerged around 2θ = 14 and 28°, respectively, indicating a facilitating effect of additives on the formation of perovskite structure, thereby enhancing the crystallinity of the film. Figure 1b shows the full width at half-maximum (fwhm) and the intensity of the (111) crystal plane. It can be observed that the peak intensity increased and fwhm decreased after the addition of MACl or MAAc, suggesting the enhanced crystallinity and grain growth of the corresponding films. Moreover, the peak intensity was higher and fwhm was smaller when MACl was added, indicating better crystallinity and larger grain size compared to the addition of MAAc. With varying concentrations of MAAc (Figure S1(a−b)), both characteristic peaks exhibited significant enhancement, with the highest peak intensity and smallest fwhm observed at 7.5%MAAc. When different amounts of MACl were added (Figure S2(a)), the intensity of perovskite characteristic peaks increased by varying degrees. Additionally, diffraction peaks from low-dimensional phases appeared in the low-angle region, especially when 1MACl was added. By comparing the fwhm and peak intensity corresponding to the (111) crystal plane (Figure S2(b)), the highest peak intensity and smallest fwhm were observed when 1.5 MACl was added, indicating the highest crystallinity and larger grain size of the film at this concentration. Besides, when 1.5MACl was added, fewer and weaker diffraction peaks of low-dimensional phases were observed, indicating reduced quantum confinement effects within the film and a higher charge transport efficiency.

To explore the effect of additives on the optical properties of the film, ultraviolet−visible (UV−vis) absorption spectroscopy was conducted. Characteristic peaks of quasi-2D perovskite structure were observed at 568, 610, and 646 nm, corresponding to n = 2, 3, and 4,[39] respectively. A feature peak of 3D perovskite appeared at 756 nm, indicating the persistence of a quasi-2D structure after additive incorporation. A noticeable increase in the absorbance intensity was observed for the film with post-additive inclusion, suggesting an enhancement in the film's optical absorption capability, likely linked to the improved film quality. Upon adding varying

https://doi.org/10.1021/acsomega.4c05875
ACS Omega 2024, 9, 46006−46016

Table 1. Performance Parameters of $(TMA)_2(MA)_4Pb_5I_{16}$ Solar Cells with Different Additives Added

additive	V_{oc}(V)	J_{sc}(mA·cm^{-2})	FF	η(%)
control	0.897 ± 0.0005 (0.907)	2.7 ± 0.02 (2.89)	0.67 ± 0.0007 (0.75)	1.65 ± 0.11[a](1.76[b])
MAAc	1.001 ± 0.00001 (1.010)	9.13 ± 0.04 (9.46)	0.56 ± 0.00001 (0.59)	5.40 ± 0.11 (5.64)
MACl	0.975 ± 0.00001 (0.980)	13.39 ± 0.04 (13.69)	0.39 ± 0.00003 (0.40)	5.09 ± 0.05 (5.34)

[a]Error values represent the standard deviation of the mean of 15 devices. [b]The best device performance values of the PSCs.

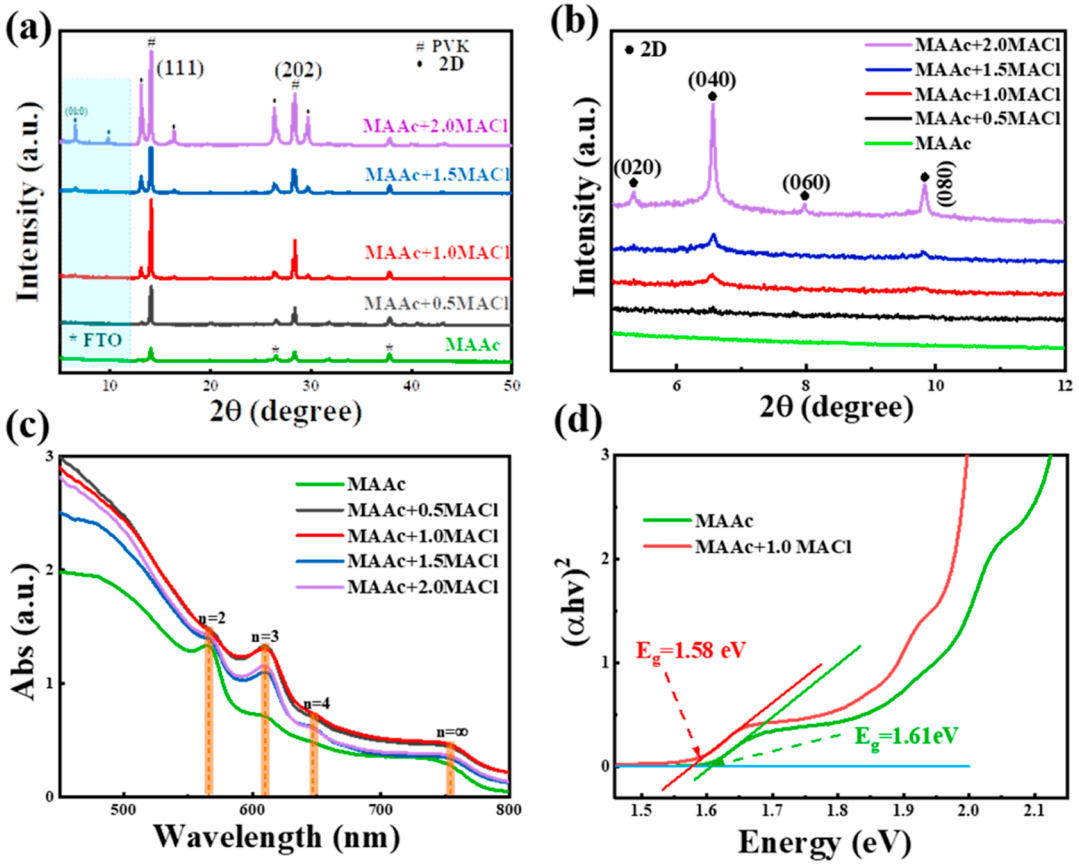

Figure 2. (a) XRD spectra of the films regulated by dual additives; (b) low-angle region (5−12°) in XRD spectra; and (c) UV−vis spectra and partial band gap schematic after dual additive regulation (d).

concentrations of MAAc (Figure S5), apart from shifts in the characteristic peak from the low-dimensional phase, a significant increase in optical absorbance was noted, with the highest absorption capacity achieved at 7.5%MAAc content. Similarly, with varying concentrations of MACl added (Figure S6), the highest absorption capacity was observed at 1.5MACl, which can be attributed to improved crystallinity and increased grain size, yet absorbance declined with continued MACl addition, correlating with a decline in film quality and consistent with SEM results.

To investigate the impact of additives on the performance of $(TMA)_2(MA)_4Pb_5I_{16}$ solar cells, devices were fabricated with $(TMA)_2(MA)_4Pb_5I_{16}$ films as the absorber layer (see the Experimental section for details). As depicted in Figure 1g, with the incorporation of additives, the device performance significantly improved with specific parameters outlined in Table 1. When different concentrations of MAAc were added (Figure 1h), the device's PCE continuously increased with MAAc addition, reaching a peak efficiency of 5.64% at 7.5% MAAc content. It should be noted that a peak-shaped feature appeared in the $J-V$ curve, which is derived from a specific distribution of ionic defects (V_I and V_{MA}) at the electron (hole) transport layer/perovskite interface, owning to the ionic movement in the perovskite layer under bias sweeping.[40] However, continued addition of MAAc led to a decline in performance, likely due to the emergence of numerous defects in the film, consistent with the SEM imaging results. As shown in Figure S7, box plots demonstrate the devices' excellent reproducibility. When different concentrations of MACl were added (Figure 1i), the highest efficiency of 5.34% was realized with 1.5MACl addition. Furthermore, from the box plots (Figure S8), it can be observed that the reproducibility of the device performance was enhanced after MACl addition.

Influence of Dual Additives on the Quality of Thin Films. From the discussion presented above, it was observed that the addition of MACl significantly increased the grain size of the $(TMA)_2(MA)_4Pb_5I_{16}$ film. However, it also induced the formation of low-dimensional perovskite phases at high additive content. On the other hand, the addition of MAAc resulted in the film with smaller grain size and excellent smoothness. Based on previous results where the best device performance was achieved with 7.5% MAAc, we further introduced the secondary additive of MACl, with the aim of achieving a compact perovskite film with large grain size.

https://doi.org/10.1021/acsomega.4c05875
ACS Omega 2024, 9, 46006−46016

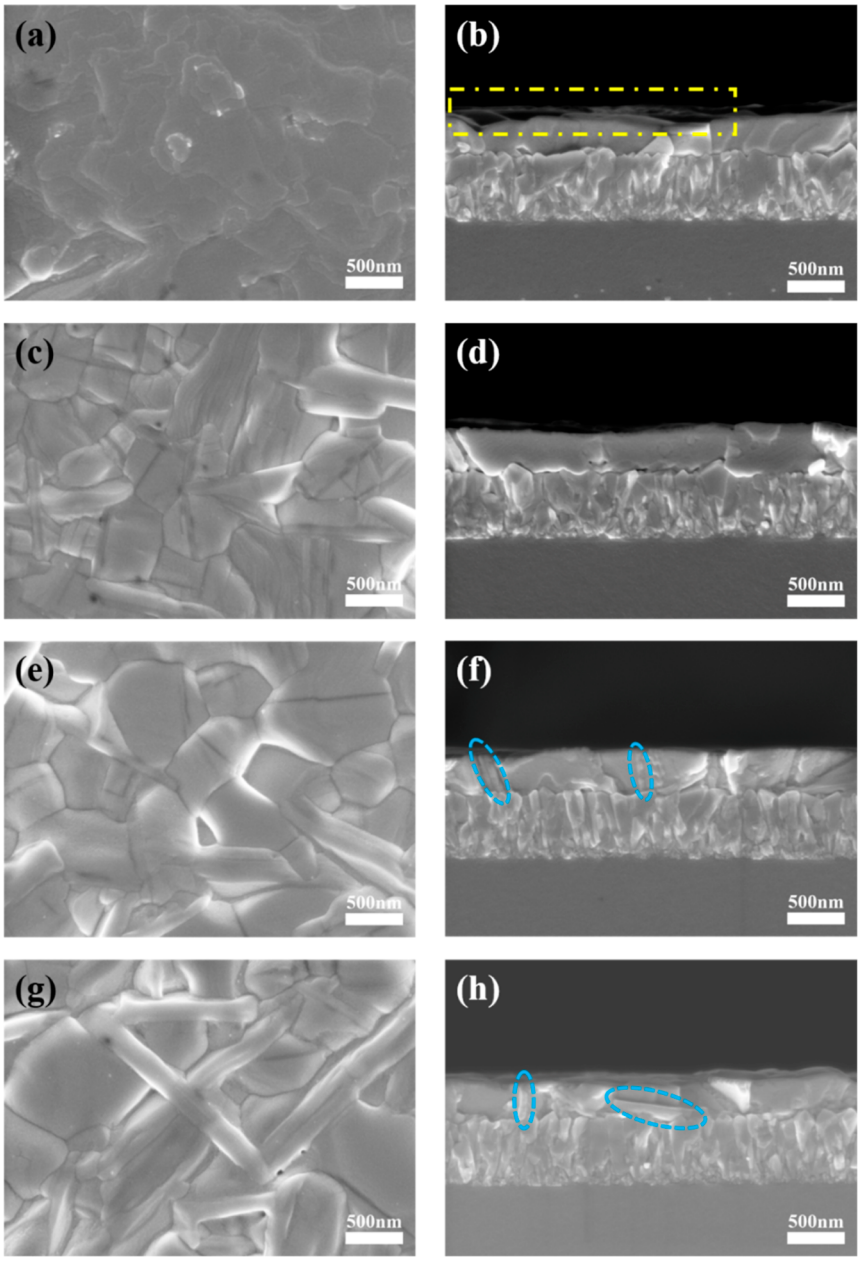

Figure 3. SEM surface morphology and cross-sectional images of dual additive regulated thin films: (a, b) MAAc + 0.5 MACl; (c, d) MAAc + 1 MACl; (e, f) MAAc + 1.5 MACl; and (g, h) MAAc + 2 MACl.

To investigate the impact of dual additives on $(TMA)_2(MA)_4Pb_5I_{16}$ thin films, XRD analysis was conducted to examine their phase structures. As depicted in Figure 2a, distinct perovskite characteristic diffraction peaks emerged in the film upon addition of the dual additives. Furthermore, under the influence of the second additive, MACl, the intensity of both characteristic peaks significantly increased, indicating an enhancement in film crystallinity due to the introduction of MACl. Additionally, as shown in Figure 2b, notable characteristic peaks from the low-dimensional phase appeared in the low-angle region, which was particularly evident with the addition of 2MACl, suggesting an excess of MACl inducing a plethora of low-dimensional perovskite phases.

To explore the impact of dual additives on the optical absorption capacity of $(TMA)_2(MA)_4Pb_5I_{16}$ thin films, UV–vis absorption measurement was performed on the films. As illustrated in Figure 2c, characteristic peaks of quasi-2D perovskite structures appeared at 566, 610, and 648 nm, corresponding to the exitonic absorption of low-dimension perovskite with n = 2, 3, and 4, respectively. A characteristic peak of the 3D perovskite was observed at 754 nm, similar to the absorption spectra obtained when MAAc or MACl was added alone. It was observed that films prepared with the addition of 0.5MACl and 1MACl exhibited stronger absorption ability, while excess MACl resulted in decreased optical absorbance and enhanced $n = 2$ excitonic absorption, indicating a decrease of perovskite crystallinity as well as an increase of existence of low-dimensional perovskite phases. As shown in Figure 2d, a comparison of the band gaps between the film with MACl and without MACl revealed that the introduction of MACl decreased the optical band gap of the

https://doi.org/10.1021/acsomega.4c05875
ACS Omega 2024, 9, 46006−46016

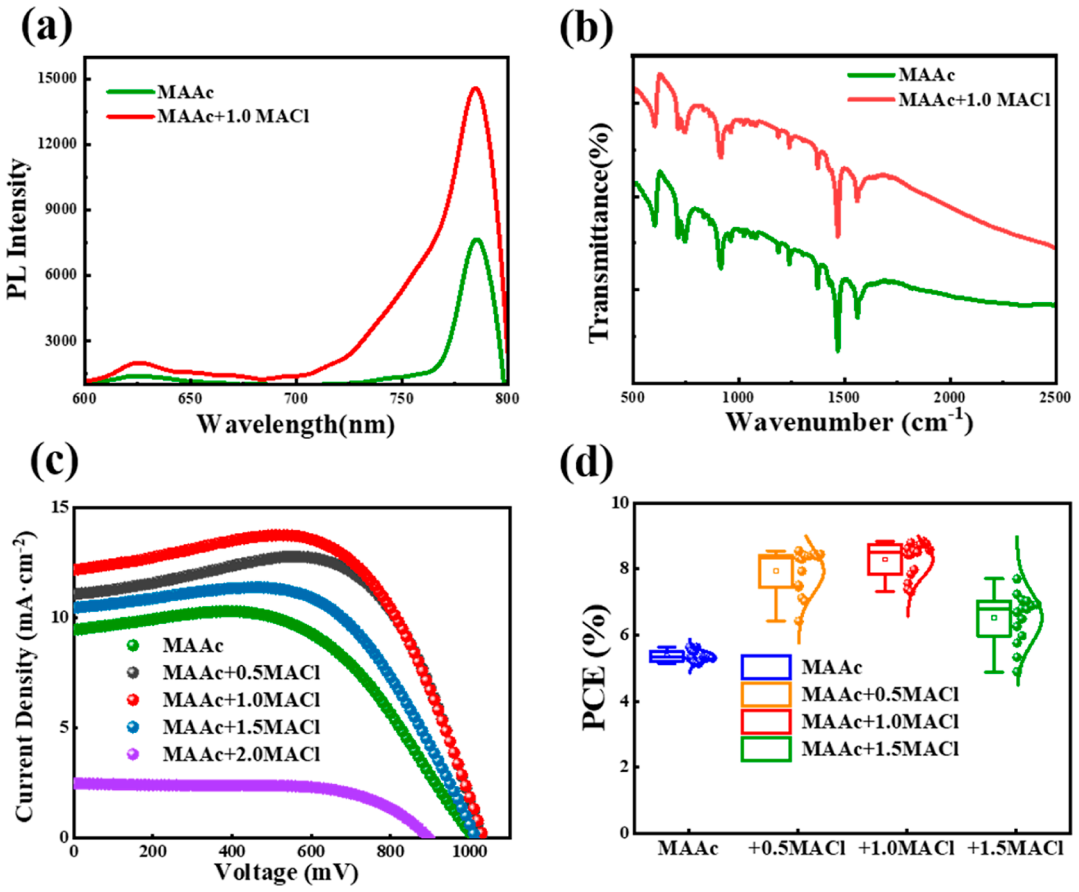

Figure 4. PL (a) and FTIR (b) spectra of $(TMA)_2(MA)_4Pb_5I_{16}$ perovskite films with single MAAc and dual MAAc + 1.0 MACl additives; PL spectra are excited from the front side at 520 nm. *J*−*V* curves (c) and box plots (d) of the $(TMA)_2(MA)_4Pb_5I_{16}$ solar cell regulated by dual additives under illumination of 1 sun.

Table 2. Performance Parameters of $(TMA)_2(MA)_4Pb_5I_{16}$ Solar Cells with Dual Additive Regulated

additive	V_{oc}(V)	J_{sc}(mA·cm^{-2})	FF	η(%)
MAAc	1.006 ± 0.002 (1.010)	9.04 ± 0.29 (9.46)	0.59 ± 0.005 (0.59)	5.36 ± 0.16[a](5.64[b])
MAAc + 0.5 MACl	1.027 ± 0.006 (1.031)	10.19 ± 1.09 (11.07)	0.75 ± 0.016 (0.75)	7.89 ± 0.76 (8.55)
MAAc + 1.0 MACl	1.029 ± 0.007 (1.034)	11.61 ± 0.75 (12.18)	0.69 ± 0.01 (0.70)	8.29 ± 0.65 (8.83)
MAAc + 1.5 MACl	1.014 ± 0.003 (1.015)	10.06 ± 0.95 (10.46)	0.64 ± 0.01 (0.63)	6.52 ± 0.75 (6.79)
MAAc + 2.0 MACl	0.885 ± 0.013 (0.896)	2.20 ± 0.26 (2.49)	0.66 ± 0.03 (0.64)	1.28 ± 0.17 (1.44)

[a]Error values represent the standard deviation of the mean of 15 devices. [b]The best device performance values of the PSCs.

film. A smaller band gap is advantageous for enhancing light harvesting ability, thereby improving device performance.

To investigate the influence of different concentrations of MACl in the dual additives on the morphology of the $(TMA)_2(MA)_4Pb_5I_{16}$ films, SEM testing was conducted, as depicted in Figure 3. Upon the addition of MACl, the grain size of the films noticeably increased, consistent with our expectations. As shown in Figure 3a, after addition of 0.5 MACl, the grain boundaries of the film were not very distinct, and the surface exhibited a covering sensation. Combined with the cross-sectional view in Figure 3b, it was observed that the grain size of the film increased but the overall surface was not sufficiently smooth, displaying significant undulations. Upon addition of 1MACl, as illustrated in Figure 3c,d, the grain size within the film further enlarged, with clear grain boundaries and tight grain-to-grain contact. The film exhibited a relatively smooth and uniform surface. On further increasing the MACl concentration, the grain size continued to increase, but some defects such as pores emerged, leading to a relative decrease in film compactness, as depicted in Figure 3e,g. Additionally, a certain amount of sheet-like grains appeared, which is particularly evident when adding 2MACl. This phenomenon may be attributed to the formation of low-dimensional 2D phases induced by the excess MACl additive. Therefore, adding 1MACl resulted in dense, smooth films with fewer low-dimensional phases, achieving high-quality films.

A PL study was conducted on $(TMA)_2(MA)_4Pb_5I_{16}$ perovskite films prepared with single and dual additives. It can be seen from Figure 4a that both $(TMA)_2(MA)_4Pb_5I_{16}$ films with single MAAc and dual MAAc + 1.0 MACl additives exhibit the main emission peak around 785 nm, corresponding to their larger n values and quasi-3D-like phase. The film with dual additives demonstrates higher PL intensity, approximately two times higher than that of the other film, indicating higher crystallinity. FTIR was used to determine the remaining additives inside the 2D perovskite films. As shown in Figure

https://doi.org/10.1021/acsomega.4c05875
ACS Omega 2024, 9, 46006−46016

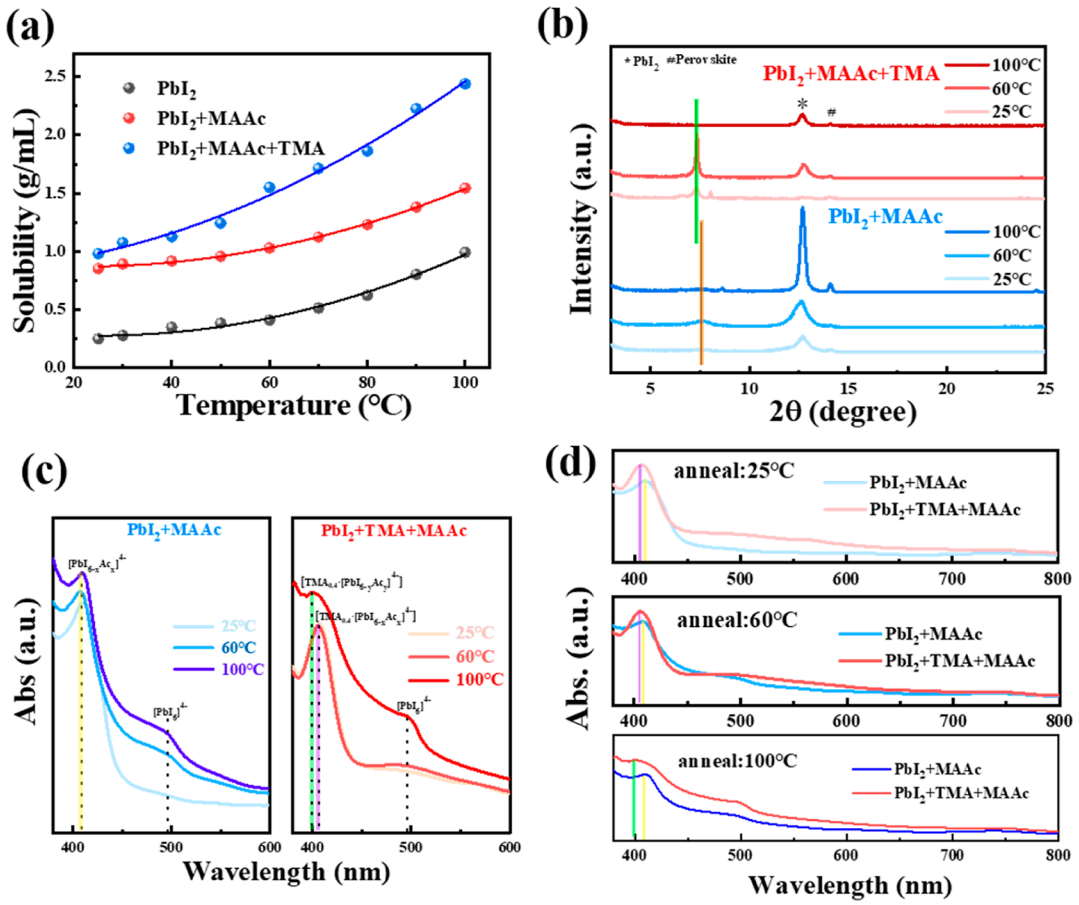

Figure 5. (a) Solubility curves of PbI_2 in pure DMF solvent and in MAAc or/and TMA-added DMF solvent; (b) XRD patterns and (c, d) UV−vis absorption spectra of PbI_2 films deposited from MAAc and TMA-added DMF solvent annealed at various temperatures.

4b, both of the films with single MAAc and dual MAAc + MACl additives after annealing show obvious C−N vibration peaks at wavenumbers between 1380 and 1550 cm^{-1}, and no C═O stretching peak is detected, indicating that the DMF solvent and MAAc additive are evaporated from the films after annealing.

Solar cells based on $(TMA)_2(MA)_4Pb_5I_{16}$ films prepared by the dual additives were fabricated. As shown in Figure 4c and Table 2, with the addition of MACl, the PCE significantly increased. When 1MACl was added, the efficiency reached a maximum of 8.83%. This enhancement was attributed to the larger grain size, improved crystallinity, and uniformity of the corresponding film, all of which lead to substantial improvements in V_{oc}, J_{sc}, and FF. However, excess MACl resulted in a deteriorated device performance, which correlated with the presence of numerous two-dimensional sheet-like crystals in the film. As depicted in Figure 4d, the box plot illustrates the performance of 15 devices, indicating good reproducibility of the cell devices after treatment with MAAc and MACl dual additives (the 2MACl component is not shown due to its significantly low efficiency and large fluctuations). The humidity stability test of the unencapsulated devices (Figure S9) reveals that the solar cell of $(TMA)_2(MA)_4Pb_5I_{16}$ with MAAc + 1.0 MACl additive maintains the highest 85% of its initial efficiency after 240 h of storage in an air environment (RT, RH = 30 ± 5%), outperforming the others.

FORMATION MECHANISM OF QUASI-2D PEROVSKITES IN THE PRESENCE OF THE DUAL ADDITIVES

MACl has been widely utilized as an additive in the preparation of perovskite films;[25,27,28,41−45] it helps to slow down the crystallization of intermediate phase $MAPbI_{3-x}Cl_x$ during perovskite formation, allowing grain growth to occur continuously during annealing and resulting in larger grain sizes, which are consistent with our experimental observations. However, there is limited research on the mechanism of MAAc as an additive. Xu et al.[30] proposed that due to the strong electron-donating ability of the C═O group in MAAc, it formed strong coordination with Pb^{2+} in the precursor solution, leading to the formation of $[PbI_{6-x}Ac_x]^{4-}$ perovskite intermediate phase, which delayed the film crystallization during annealing, resulting in larger grains. However, this explanation does not align with our results, possibly due to the use of TMA as the spacer cation, which has a unique S atom that coordinates with Pb^{2+} in the precursor solution. To investigate the influence of MAAc on the crystallization process of $(TMA)_2(MA)_4Pb_5I_{16}$ films, we elaborately studied the interaction between MAAc, TMA, and Pb^{2+}.

The solubility of PbI_2 in DMF and in MAAc and/or TMA-added DMF solvent at different temperatures was tested (see Experimental section for testing methods). As shown in Figure 5a, the solubility increases with temperature, and the addition of MAAc significantly enhances the solubility of PbI_2, indicating a strong interaction between Ac- and Pb^{2+}. When

https://doi.org/10.1021/acsomega.4c05875
ACS Omega 2024, 9, 46006−46016

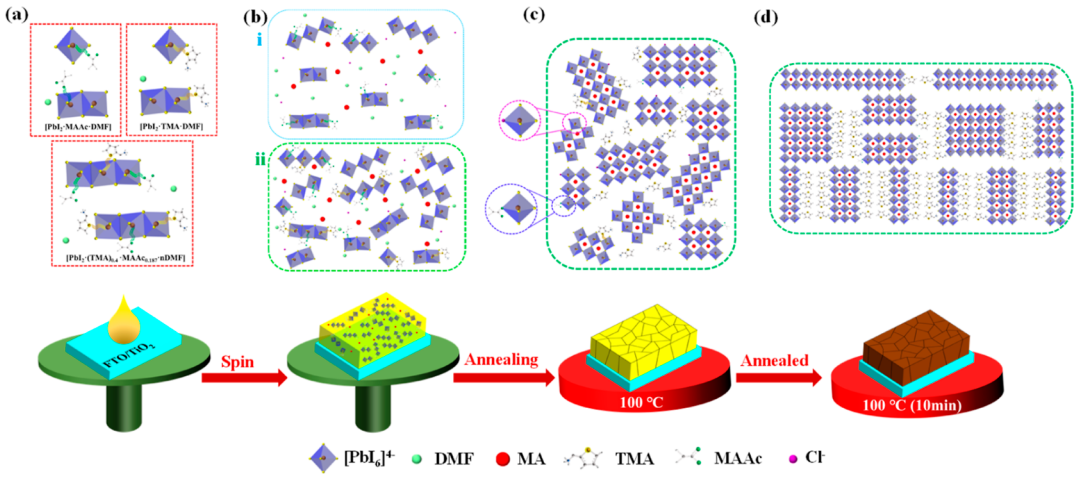

Figure 6. Schematic diagram of the formation mechanism of $(TMA)_2(MA)_4Pb_5I_{16}$ thin films using additives MAAc and MACl, (a) Complexes containing $[PbI_6]^{4-}$ octahedra with sharing edges form in the perovskite precursor, (b) complexes decompose into nuclei with corner-shared $[PbI_6]^{4-}$ octahedra during spin-coating, (c) nuclei grow into the perovskite matrix with annealing, and (d) formation of orientated perovskite films with high crystallinity and large grain.

both MAAc and TMA are added to the solvent, the solubility of PbI_2 further accelerates and increases. At 100 °C, the solubility of PbI_2 in MAAc and TMA-contained solvent is 2.5 times higher than that of PbI_2 in MAAc-added DMF, suggesting that TMA forms new complexes with MAAc and PbI_2, leading to further enhancement of PbI_2 solubility.

In order to further study the interaction between PbI_2, MAAc, and TMA, PbI_2 films were deposited from different precursors. The precursor solutions were prepared by adding MAAc and MAAc + TMA into 1 M PbI_2 DMF solution, respectively, with the same molar ratios of MAAc and TMA^+ to Pb^{2+} as that of the corresponding $(TMA)_2(MA)_4Pb_5I_{16}$ precursor. XRD and UV−vis absorption tests were conducted on the films annealed at various temperatures for 10 min. As shown in Figure 5b, regardless of the annealing temperature and composition of the precursor, the main phase of the films is PbI_2. When annealed at 100 °C, the films deposited from both precursors exhibit weak perovskite diffraction peaks at around 14° due to the existence of MAAc in the solution. In the absence of TMA, besides the characteristic peak of PbI_2 at 12.6°, a new diffraction peak appears at 7.5°, possibly due to the formation of a complex between MAAc and PbI_2, such as the reported complex ($[PbI_2{\cdot}(MAAc)_{0.187}{\cdot}mDMF]$, where m is uncertain).[30] As the annealing temperature reaches 60 °C, the intensity of the complex peak increases, and after annealing at 100 °C, the complex gradually decomposes, leading to the formation of highly crystalline PbI_2 as Ac^- volatilizes. Upon the addition of TMA + MAAc, new diffraction peaks appear at 7.3 and 8.0° in the XRD spectra, indicating the formation of a new complex among the three components, and at 25 °C, this complex shows obvious diffraction peaks. Considering the molar ratios of TMA, MAAc, and PbI_2 in DMF, the complex is defined as $[(TMA)_{0.4}{\cdot}PbI_2{\cdot}(MAAc)_{0.187}{\cdot}n$ DMF] (where n is uncertain). The intensity of the corresponding peaks increases when the annealing temperature rises to 60 °C. Further increasing the annealing temperature to 100 °C leads to the decomposition of the complex, as revealed by the disappearance of peak indicated by the vertical line in Figure 5b. From the FTIR spectra of different PbI_2 films annealed at various temperatures (Figure S10), we can see that when TMA + DMF was added into the precursor, new vibration bands appear in 1400−1600 cm^{-1}, hinting an interaction between DMF/MAAc/TMA and PbI_2 via Lewis acid−base adduct formation.

Figure 5c depicts the UV−vis absorption spectra of the films deposited from precursors with MAAc or MAAc + TMA added into a 1 M PbI_2 solution. With increasing annealing temperature, characteristic absorption peaks ascribing to $[PbI_6]^{4-}$ appeared in all films.[46] Under the influence of MAAc, a distinct absorption peak emerged at 409 nm, which could be attributed to the complex that is defined as $[PbI_{6-x}Ac_x]^{4-}$ and is consistent with XRD results. Upon combined interaction of MAAc and TMA, at lower temperatures (<60 °C), a characteristic absorption peak appeared at 406 nm, with reduced intensity of $[PbI_6]^{4-}$ peaks, indicating predominant presence of Pb^{2+} in the complex form. Considering the molar ratio of TMA^+ to Pb^{2+} in solution, the formula of the complex is denoted as $[TMA_{0.4}{\cdot}PbI_{6-x}Ac_x]^{4-}$. With a further increase in annealing temperature, Ac^- further evaporated, manifesting distinct $[PbI_6]^{4-}$ characteristic peaks and new absorption peaks at 400 nm, defined as $[TMA_{0.4}{\cdot}PbI_{6-y}Ac_y]^{4-}$. As shown in Figure 5d, noticeable differences in the absorption peaks were observed at the same annealing temperature between PbI_2 films with and without TMA, confirming the formation of a new complex with TMA ($[(TMA)_{0.4}{\cdot}PbI_2{\cdot}(MAAc)_{0.187}{\cdot}n$ DMF]).

After the above analysis, the mechanism by which the dual additives (MAAc + MACl) enhance the quality of $(TMA)_2(MA)_4Pb_5I_{16}$ perovskite films is proposed. In the precursor, as shown in Figure 6a, Pb^{2+} and I^- typically connect as $[PbI_6]^{4-}$ octahedra with sharing edges. However, when the solution contains MAAc and TMA, the strong interactions of carbonyl groups from Ac^- and sulfur atom from TMA with Pb^{2+} lead to the formation of complexes of $[(TMA)_{0.4}{\cdot}PbI_2{\cdot}(MAAc)_{0.187}{\cdot}n$ DMF], which was already witnessed by the XRD pattern, UV−vis absorption, and FTIR spectra in Figure 5 and Figure S10. These complexes significantly enhance the solubility of PbI_2 in DMF, as evidenced in Figure 5a. As shown in Figure 6b, during spin-coating, as DMF and MAAc evaporate, the complexes decompose into corner-shared $[PbI_6]^{4-}$ octahedra, which facilitate nucleation of the perovskite. Therefore, compared to the solution without the

https://doi.org/10.1021/acsomega.4c05875
ACS Omega 2024, 9, 46006−46016

complex (Figure 6b-i), the solution with the complex has more nucleation points during the spin-coating process (Figure 6b-ii). When annealed, as shown in Figure 6c, DMF and MAAc evaporate, and the perovskite nuclei continue to grow. The rapid formation of numerous nuclei leads to dense films with fine grains, where defects like pores disappear under the influence of MAAc, improving film quality.

Upon further addition of MACl, as reported in the literature,[28] the introduction of Cl^- leads to the formation of intermediate phases like $MAPbI_{3-x}Cl_x$ during film annealing, which slows down the crystallization of perovskite films. With prolonged annealing, Cl^- ions evaporate from the deposit, forming orientated perovskite films with high crystallinity and large grain, as shown in Figure 6(d). When both MAAc and MACl are used as additives, MAAc helps to form complexes to facilitate nucleation nuclei, while MACl exerts a synergistic effect on promoting crystal growth, resulting in dense films with large grains. Therefore, perovskite films ($(TMA)_2(MA)_4Pb_5I_{16}$) prepared under the combined effect of MAAc and MACl exhibit much improved crystallinity and well-defined morphology, leading to devices with excellent performance.

CONCLUSIONS

In this study, TMA was selected as the spacer cation to prepare $(TMA)_2MA_4Pb_5I_{16}$ perovskite films, and the film quality was regulated by adding MACl and MAAc. It was found that adding MACl resulted in a film of larger grains with a PCE of 5.34%, while excessive MACl led to the formation of low-dimensional phases. Adding 7.5%MAAc improved film quality with a PCE of 5.64%, although excessive MAAc caused defects, such as pores and smaller grains. A high-quality $(TMA)_2MA_4Pb_5I_{16}$ perovskite film with a champion PCE of 8.86% was achieved when both MACl and MAAc were used as additives. Studies on the formation mechanism revealed that TMA and MAAc could form a complex $[(TMA)_{0.4}{\cdot}PbI_2{\cdot}(MAAc)_{0.187}{\cdot}n$ DMF] (where n is an undetermined value) with PbI_2 in the solution, which helps to promote the formation of nuclei. MACl as the secondary additive exerts a synergistic effect on promoting crystal growth, resulting in dense films with large grains and high crystallinity. This study proposes new ideas for the use of dual additives and the role of additives in film formation, providing new insights for the preparation of high-quality 2D perovskite films.

ASSOCIATED CONTENT

Supporting Information

The Supporting Information is available free of charge at https://pubs.acs.org/doi/10.1021/acsomega.4c05875.

XRD patterns, SEM images, UV−vis absorption spectra, FTIR spectra, box plots of solar cell PCE, parameters of solar cell devices, and normalized PCEs versus time for unencapsulated devices (PDF)

AUTHOR INFORMATION

Corresponding Author

Xiaoyan Gan − *Sanya Science and Education Innovation Park, Wuhan University of Technology, Sanya 572024, China; School of Materials Science and Engineering, Wuhan University of Technology, Wuhan 430070, China;* orcid.org/0000-0002-0352-7428; Email: ganxiaoyan@whut.edu.cn

Authors

Kegui Li − *School of Materials Science and Engineering, Wuhan University of Technology, Wuhan 430070, China*

Longtao Du − *School of Materials Science and Engineering, Wuhan University of Technology, Wuhan 430070, China*

Ruoqi Wang − *School of Materials Science and Engineering, Wuhan University of Technology, Wuhan 430070, China*

Yuge Chang − *School of Materials Science and Engineering, Wuhan University of Technology, Wuhan 430070, China*

Liling Guo − *School of Materials Science and Engineering, Wuhan University of Technology, Wuhan 430070, China*

Hanxing Liu − *International School of Materials Science and Engineering, Wuhan University of Technology, Wuhan 430070, China;* orcid.org/0000-0002-8625-4866

Complete contact information is available at: https://pubs.acs.org/10.1021/acsomega.4c05875

Author Contributions

Xiaoyan Gan: conceptualization, methodology, software, resources. Kegui Li: carried out laboratory research, investigation, data curation, writing—original draft, writing—review and editing, visualization. Longtao Du: carried out laboratory research, validation. Ruoqi Wang: carried out laboratory research, formal analysis. Yuge Chang: carried out laboratory research, formal analysis. Liling Guo: supervision, project administration. Hanxing Liu: supervision, resources.

Funding

This work was financially supported by the National Natural Science Foundation of China (51772228) and the open fund of Sanya Science and Education Innovation Park (2022KF0008).

Notes

The authors declare no competing financial interest.

REFERENCES

(1) Jung, E. H.; Jeon, N. J.; Park, E. Y.; Moon, C. S.; Shin, T. J.; Yang, T.-Y.; Noh, J. H.; Seo, J. Efficient, stable and scalable perovskite solar cells using poly(3-hexylthiophene). *Nature* **2019**, *567* (7749), 511−515.

(2) Peng, W.; Mao, K.; Cai, F.; Meng, H.; Zhu, Z.; Li, T.; Yuan, S.; Xu, Z.; Feng, X.; Xu, J.; McGehee, M. D.; Xu, J. Reducing nonradiative recombination in perovskite solar cells with a porous insulator contact. *Science* **2023**, *379* (6633), 683−690.

(3) Wang, Z.; Shi, Z.; Li, T.; Chen, Y.; Huang, W. Stabilität vonPerowskit-Solarzellen: Einfluss der Substitution von A-Kation und XAnion. *Angew. Chem.* **2017**, *129*, 1210−1233.

(4) Yin, X.; Wang, C.; Zhao, D.; Shrestha, N.; Grice, C. R.; Guan, L.; Song, Z.; Chen, C.; Li, C.; Chi, G.; Zhou, B.; Yu, J.; Zhang, Z.; Ellingson, R. J.; Zhou, J.; Yan, Y.; Tang, W. Binary hole transport materials blending to linearly tune HOMO level for high efficiency and stable perovskite solar cells. *Nano Energy* **2018**, *51*, 680−687.

(5) Liu, X.; Yu, H.; Yan, L.; Dong, Q.; Wan, Q.; Zhou, Y.; Song, B.; Li, Y. Triple Cathode Buffer Layers Composed of PCBM, C60, and LiF for High-Performance Planar Perovskite Solar Cells. *ACS Appl. Mater. Interfaces* **2015**, *7* (11), 6230−6237.

(6) Smith, I. C.; Hoke, E. T.; Solis-Ibarra, D.; McGehee, M. D.; Karunadasa, H. I. A Layered Hybrid Perovskite Solar-Cell Absorber with Enhanced Moisture Stability. *Angew. Chem., Int. Ed.* **2014**, *53* (42), 11232−11235.

(7) Niu, T.; Ren, H.; Wu, B.; Xia, Y.; Xie, X.; Yang, Y.; Gao, X.; Chen, Y.; Huang, W. Reduced-Dimensional Perovskite Enabled by Organic Diamine for Efficient Photovoltaics. *J. Phys. Chem. Lett.* **2019**, *10* (10), 2349−2356.

(8) Zhang, X.; Ren, X.; Liu, B.; Munir, R.; Zhu, X.; Yang, D.; Li, J.; Liu, Y.; Smilgies, D.-M.; Li, R.; Yang, Z.; Niu, T.; Wang, X.; Amassian,

A.; Zhao, K.; Liu, S. Stable high efficiency two-dimensional perovskite solar cells via cesium doping. *Energy Environ. Sci.* **2017**, *10* (10), 2095−2102.
(9) Zhang, F.; Kim, D. H.; Lu, H.; Park, J.-S.; Larson, B. W.; Hu, J.; Gao, L.; Xiao, C.; Reid, O. G.; Chen, X.; Zhao, Q.; Ndione, P. F.; Berry, J. J.; You, W.; Walsh, A.; Beard, M. C.; Zhu, K. Enhanced Charge Transport in 2D Perovskites via Fluorination of Organic Cation. *J. Am. Chem. Soc.* **2019**, *141* (14), 5972−5979.
(10) Mao, L.; Stoumpos, C. C.; Kanatzidis, M. G. Two-Dimensional Hybrid Halide Perovskites: Principles and Promises. *J. Am. Chem. Soc.* **2019**, *141* (3), 1171−1190.
(11) Leung, T. L.; Ahmad, I.; Syed, A. A.; Ng, A. M. C.; Popović, J.; Djurišić, A. B. Stability of 2D and quasi-2D perovskite materials and devices. *Commun. Mater.* **2022**, *3* (1), 63.
(12) Xu, Y.; Wen, X.; Zheng, G.; Wang, Y.; Li, Y.; Li, B.; Yang, Y.; Liang, J.; Chen, D.; Hou, L.; Cai, W.; Qing, J. High-Quality Lead Acetate-Based Ruddlesden-Popper Perovskite Films for Efficient Solar Cells. *Sol. RRL* **2023**, *7* (12), 202300111.
(13) Tsai, H.; Nie, W.; Blancon, J.-C.; Stoumpos, C. C.; Asadpour, R.; Harutyunyan, B.; Neukirch, A. J.; Verduzco, R.; Crochet, J. J.; Tretiak, S.; Pedesseau, L.; Even, J.; Alam, M. A.; Gupta, G.; Lou, J.; Ajayan, P. M.; Bedzyk, M. J.; Kanatzidis, M. G.; Mohite, A. D. High-efficiency two-dimensional Ruddlesden-Popper perovskite solar cells. *Nature* **2016**, *536* (7616), 312−316.
(14) Zhang, X.; Yang, T.; Ren, X.; Zhang, L.; Zhao, K.; Liu, S. Film Formation Control for High Performance Dion-Jacobson 2D Perovskite Solar Cells. *Adv. Energy Mater.* **2021**, *11* (19), 202002733.
(15) Wu, H. T.; Lian, X. M.; Tian, S. X.; Zhang, Y. Z.; Qin, M. C.; Zhang, Y. Y.; Wang, F. Y.; Lu, X. H.; Wu, G.; Chen, H. Z. Additive assisted hot-casting free fabrication of Dion-Jacobson 2D perovskite solar cell with efficiency beyond 16%. In *47th IEEE Photovoltaic Specialists Conference (PVSC)*; IEEE, 2020; pp 93−95.
(16) Lai, H. T.; Lu, D.; Xu, Z. Y.; Zheng, N.; Xie, Z. Q.; Liu, Y. S. Organic-Salt-Assisted Crystal Growth and Orientation of Quasi-2D Ruddlesden−Popper Perovskites for Solar Cells with Efficiency over 19%. *Adv. Mater.* **2020**, *32* (33), 202001470.
(17) Liang, J.; Zhang, Z.; Xue, Q.; Zheng, Y.; Wu, X.; Huang, Y.; Wang, X.; Qin, C.; Chen, Z.; Chen, C.-C. A finely regulated quantum well structure in quasi-2D Ruddlesden−Popper perovskite solar cells with efficiency exceeding 20%. *Energy Environ. Sci.* **2022**, *15* (1), 296−310.
(18) Liang, J.; Sun, A.; Zhang, Z.; Zheng, Y.; Wu, X.; Tian, C.; Chen, Z.; Chen, C.-C. Volatile 2-Thiophenemethylammonium and Its Strongly Bonded Condensation Product for Stabilizing α-FAPbI3 in Sequential-Deposited Solar Cells. *ACS Mater. Lett.* **2023**, *5* (5), 1395−1400.
(19) Qin, Y.; Zhong, H.; Intemann, J. J.; Leng, S.; Cui, M.; Qin, C.; Xiong, M.; Liu, F.; Jen, A. K. Y.; Yao, K. Coordination Engineering of Single-Crystal Precursor for Phase Control in Ruddlesden-Popper Perovskite Solar Cells. *Adv. Energy Mater.* **2020**, *10* (16), 201904050.
(20) Hu, J.-F.; Chen, G.; Yu, S.-Z.; Lin, Y.-X.; Wang, K.-Y.; Li, Z.-W.; Zhang, G.-D.; Pan, T.-F.; Li, Y.-J.; Li, M.-J.; Xia, Y.-D.; Lv, Y.-F.; Chen, Y.-H. Efficient micrometer-scale thick-film perovskite solar cells with superior stability. *Rare Metals* **2024**, *43* (4), 1647−1657.
(21) Lv, Y.; Li, Y.; Zhou, Y.; Liu, J.; Wang, J.; Lin, Y.; Hu, J.; Pan, T.; Li, Y.; Wang, K.; Xia, Y.; Shi, W.; Chen, Y. Efficient and Stable β-$CsPbI_3$ Solar Cells through Solvent Engineering with Methylamine Acetate Ionic Liquid. *ACS Appl. Mater. Interfaces* **2023**, *15* (24), 29236−29243.
(22) Chao, L.; Xia, Y.; Li, B.; Xing, G.; Chen, Y.; Huang, W. Room-Temperature Molten Salt for Facile Fabrication of Efficient and Stable Perovskite Solar Cells in Ambient Air. *Chem* **2019**, *5* (4), 995−1006.
(23) Liao, K.; Li, C.; Xie, L.; Yuan, Y.; Wang, S.; Cao, Z.; Ding, L.; Hao, F. Hot-Casting Large-Grain Perovskite Film for Efficient Solar Cells: Film Formation and Device Performance. *Nano-Micro Lett.* **2020**, *12* (1), 156.
(24) Wang, F.; Ge, C.; Zhou, X.; Liang, X.; Duan, D.; Lin, H.; Zhu, Q.; Hu, H. Manipulation of Crystallization Kinetics for Perovskite Photovoltaics Prepared Using Two-Step Method. *Crystals* **2022**, *12* (6), 815.
(25) Wu, G.; Cai, M.; Cao, Y.; Li, Z.; Zhang, Z.; Yang, W.; Chen, X.; Ren, D.; Mo, Y.; Yang, M.; Liu, X.; Dai, S. Enlarging grain sizes for efficient perovskite solar cells by methylamine chloride assisted recrystallization. *J. Energy Chem.* **2022**, *65*, 55−61.
(26) Liu, Z.; Liu, T.; Li, M.; He, T.; Guo, G.; Liu, P.; Chen, T.; Yang, J.; Qin, C.; Dai, X.; Yuan, M. Eliminating Halogen Vacancies Enables Efficient MACL-Assisted Formamidine Perovskite Solar Cells. *Adv. Sci.* **2024**, *11* (7), 202306280.
(27) Lehner, L. E.; Demchyshyn, S.; Frank, K.; Minenkov, A.; Kubicki, D. J.; Sun, H.; Hailegnaw, B.; Putz, C.; Mayr, F.; Cobet, M.; Hesser, G.; Schöfberger, W.; Sariciftci, N. S.; Scharber, M. C.; Nickel, B.; Kaltenbrunner, M. Elucidating the Origins of High Preferential Crystal Orientation in Quasi-2D Perovskite Solar Cells. *Adv. Mater.* **2023**, *35* (5), 202208061.
(28) Zuo, W.-W.; Yang, Y.-G.; Fu, W.-F.; Li, M.; Malekshahi Byranvand, M.; Di Girolamo, D.; Pascual, J.; Li, M.-Q.; Li, L.-N.; Abate, A.; Saliba, M.; Wang, Z.-K. In Situ Methylammonium Chloride-Assisted Perovskite Crystallization Strategy for High-Performance Solar Cells. *ACS Mater. Lett.* **2022**, *4* (3), 448−456.
(29) Lai, H.; Kan, B.; Liu, T.; Zheng, N.; Xie, Z.; Zhou, T.; Wan, X.; Zhang, X.; Liu, Y.; Chen, Y. Two-Dimensional Ruddlesden−Popper Perovskite with Nanorod-like Morphology for Solar Cells with Efficiency Exceeding 15%. *J. Am. Chem. Soc.* **2018**, *140* (37), 11639−11646.
(30) Xu, T.; Lu, S.; Wang, Y.; Gan, X.; Guo, L.; Liu, H. Optimization of multilayered Ruddlesden-Popper perovskite with 4-bromophenylethylamine by ionic liquid for solar cell applications. *J. Mater. Sci.* **2022**, *57* (16), 7896−7908.
(31) Lu, S.; Li, K.; Zhen, R.; Xiang, M.; Gan, X.; Guo, L.; Liu, H. Incorporating formamidinium into 4-fluoro-phenethylammonium based quasi-2D perovskite films and their application in n-i-p perovskite solar cells. *Opt. Mater.* **2023**, *136*, 113453.
(32) Ma, W.; Zhang, Z.; Liu, Y.; Gao, H.; Mao, Y. Highly efficient and stable quasi two-dimensional perovskite solar cells via synergistic effect of dual additives. *J. Colloid Interface Sci.* **2023**, *646*, 922−931.
(33) Fu, W.; Wang, J.; Zuo, L.; Gao, K.; Liu, F.; Ginger, D. S.; Jen, A. K. Y. Two-Dimensional Perovskite Solar Cells with 14.1% Power Conversion Efficiency and 0.68% External Radiative Efficiency. *ACS Energy Lett.* **2018**, *3* (9), 2086−2093.
(34) Yan, Y.; Yu, S.; Honarfar, A.; Pullerits, T.; Zheng, K.; Liang, Z. Benefiting from Spontaneously Generated 2D/3D Bulk-Heterojunctions in Ruddlesden-Popper Perovskite by Incorporation of S-Bearing Spacer Cation. *Adv. Sci.* **2019**, *6* (14), 201900548.
(35) Zhou, T.; Lai, H.; Zhang, X.; Lu, D.; Lai, H.; Wan, X.; Liu, Y.; Chen, Y.; Zhang, X.; Liu, Y.; Chen, Y.; et al. Highly Efficient and Stable Solar Cells Based on Crystalline Oriented 2D/3D Hybrid Perovskite. *Adv. Mater.* **2019**, *31* (32), 201901242.
(36) Ni, C.; Huang, Y.; Zeng, T.; Chen, D.; Chen, H.; Wei, M.; Johnston, A.; Proppe, A. H.; Ning, Z.; Sargent, E. H.; Hu, P.; Yang, Z. Thiophene Cation Intercalation to Improve Band-Edge Integrity in Reduced-Dimensional Perovskites. *Angew. Chem., Int. Ed.* **2020**, *59* (33), 13977−13983.
(37) Liang, J.; Zhang, Z.; Huang, Y.; Xue, Q.; Zheng, Y.; Wu, X.; Tian, C.; Zhang, Y.; Wang, Y.; Chen, Z.; Chen, C.-C. Volatile 2D Ruddlesden-Popper Perovskite: A Gift for α-Formamidinium Lead Triiodide Solar Cells. *Adv. Funct. Mater.* **2022**, *32* (51), 202207177.
(38) Li, K.; Gan, X.; Zheng, R.; Zhang, H.; Xiang, M.; Dai, S.; Du, D.; Zhang, F.; Guo, L.; Liu, H. Comparative Analysis of Thiophene-Based Interlayer Cations for Enhanced Performance in 2D Ruddlesden-Popper Perovskite Solar Cells. *ACS Appl. Mater. Interfaces* **2024**, *16* (6), 7161−7170.
(39) Zhang, Y. Y.; Keshavarz, M.; Debroye, E.; Fron, E.; Rodríguez González, M. C.; Naumenko, D.; Amenitsch, H.; Van de Vondel, J.; De Feyter, S.; Heremans, P.; Roeffaers, M. B. J.; Qiu, W. M.; Pradhan, B.; Hofkens, J. Two-dimensional perovskites with alternating cations in the interlayer space for stable light-emitting diodes. *Nanophotonics* **2021**, *10* (8), 2145−2156.

https://doi.org/10.1021/acsomega.4c05875
ACS Omega 2024, 9, 46006−46016

(40) Wu, F.; Bahrami, B.; Chen, K.; Mabrouk, S.; Pathak, R.; Tong, Y.; Li, X.; Zhang, T.; Jian, R.; Qiao, Q. Bias-Dependent Normal and Inverted J−V Hysteresis in Perovskite Solar Cells. *ACS Appl. Mater. Interfaces* **2018**, *10* (30), 25604−25613.
(41) Kim, M.; Kim, G.-H.; Lee, T. K.; Choi, I. W.; Choi, H. W.; Jo, Y.; Yoon, Y. J.; Kim, J. W.; Lee, J.; Huh, D.; Lee, H.; Kwak, S. K.; Kim, J. Y.; Kim, D. S. Methylammonium Chloride Induces Intermediate Phase Stabilization for Efficient Perovskite Solar Cells. *Joule* **2019**, *3* (9), 2179−2192.
(42) Zhang, X.; Qiu, W. M.; Song, W. Y.; Hawash, Z.; Wang, Y. X.; Pradhan, B.; Zhang, Y. Y.; Naumenko, D.; Amenitsch, H.; Moons, E.; Merckx, T.; Aguirre, A.; Abdulraheem, Y.; Aernouts, T.; Zhan, Y. Q.; Kuang, Y. H.; Hofkens, J.; Poortmans, J. An Integrated Bulk and Surface Modification Strategy for Gas-Quenched Inverted Perovskite Solar Cells with Efficiencies Exceeding 22%. *Sol. RRL* **2022**, *6* (6), 2200053.
(43) Takahashi, S.; Uchida, S.; Segawa, H. Effect of Chloride Incorporation on the Intermediate Phase and Film Morphology of Methylammonium Lead Halide Perovskites. *ACS Omega* **2023**, *8* (45), 42711−42721.
(44) Cuzzupe, D. T.; Oz, S. D.; Ling, J.; Illing, E.; Seewald, T.; Jose, R.; Olthof, S.; Fakharuddin, A.; Schmidt-Mende, L. Understanding the Methylammonium Chloride-Assisted Crystallization for Improved Performance of Lead-Free Tin Perovskite Solar Cells. *Sol. RRL* **2023**, *7* (24), 2300770.
(45) Wang, Z.; Liu, L.; Liu, X. D.; Song, D. D.; Shi, D.; Wu, S. H.; Tong, Y. W.; Ren, H.; Li, M. J.; Zheng, Y. H.; Zhao, D. W. Uncovering synergistic effect of chloride additives for efficient quasi-2D perovskite solar cells. *Chem. Eng. J.* **2022**, *432*, 134367.
(46) Zhong, Y.; Liu, G.; Su, Y.; Sheng, W.; Gong, L.; Zhang, J.; Tan, L.; Chen, Y. Diammonium Molecular Configuration-Induced Regulation of Crystal Orientation and Carrier Dynamics for Highly Efficient and Stable 2D/3D Perovskite Solar Cells. *Angew. Chem., Int. Ed.* **2022**, *61* (5), 202114588.

https://doi.org/10.1021/acsomega.4c05875
ACS Omega 2024, 9, 46006−46016